Dynamical adiabatic theory of atomic collisions: The global structure of dynamical adiabatic potential energy curves

T. P. Grozdanov[*]

Institute of Physics, University of Belgrade, Pregrevica 118, 11080 Belgrade, Serbia

E. A. Solov'ev

Bogoliubov Laboratory of Theoretical Physics, Joint Institute for Nuclear Research, 141980 Dubna, Moscow Region, Russia

The concept of dynamical adiabatic states, originally proposed to describe one-electron atom(ion)-ion collision systems is developed and the properties of the corresponding dynamical adiabatic potential energy curves are studied for a complete range of internuclear separations R. The advantages of a dynamical adiabatic basis are threefold. First, it is compatible with the boundary conditions, whereas in standard adiabatic two-Coulomb center basis we have nonvanishing inelastic transitions when internuclear distance $R \to \infty$. Second, rotational transitions are transformed into radial transitions via a type of hidden crossings in contrast with the standard adiabatic basis, where these transitions could only be included by numerical close-coupling calculations. And third, the ionization process can be described using a basis of the complete discrete orthogonal wave packets, which is much more satisfactory for the process compared with the standard adiabatic approach where the continuum states which have no direct physical meaning are employed. Results of the calculation for the $(HeH)^{2+}$ quasimolecular system are presented and discussed. Comparison is made with previous results derived by perturbation theory in the united-atom and separated atoms limits.

I. INTRODUCTION

The adiabatic approximation for slow atomic collisions is valid for impact energies up to about 10 KeV/nucleon. This interval covers many processes occurring in the natural world, including ionized stellar atmospheres and TOKAMAK fusion plasmas. It has been extensively developed during the past 50 years. Initially, the description of inelastic processes was restricted by the transitions via narrow avoided crossings between molecular potential energy curves (PEC) corresponding to states located on different nuclei. The splitting of the energies at the point of avoided crossing is determined by the under-barrier penetration of an electron from Coulomb well of one nucleus to the other and is exponentially small with respect to the inverse of Planck constant $\hbar$. However, such avoided crossings are absent, for example, in the quasimolecular system H_2^+. In 1981 a new mechanism of nonadiabatic transitions was discovered and attributed to the so-called "hidden crossings" [1], which are not visible on the plot of the PEC for real internuclear separations R. They can be verified by direct numerical calculation in the complex R-plain as branch points of the PEC $E(R)$ and appear when the real energy level $E_n(R)$ touches the top of an effective electron potential, that is the electron trajectory collapses into unstable periodic orbit. Their splitting is determined by the Lyapunov index and is proportional to $\hbar$. Only "hidden-crossings" together with the "avoided crossings" and rotational transitions describe a complete set of inelastic transitions in the standard adiabatic approach.

It is a well-known fact in the theory of ion-atom collisions that when using an expansion of the wavefunction in terms of adiabatic eigenstates of the quasimolecule formed during the collision, the problem of obeying the proper boundary conditions occurs. Thus, in the impact-parameter formulation of the theory (that is, when the motion of the nuclei is described classically), in order to obtain a Galilean invariant theory, it is necessary to attach to each of the basis functions the so-called "electron translation factors" (for a review see Ref. [2]). An elegant solution to this problem is the method of nonstationary scaling of the length (NSSL), proposed originally by one of the authors [3,4]. In this approach, the problem is reduced to the one in which the nuclei are at rest, but additional dynamical interactions appear in the electronic Hamiltonian [5]. More recently, the NSSL has been successfully used to treat the problems of electron-atom(molecule) collisions [6] and the interaction of atoms and molecules with radiation fields [7,8].

In the case of ion-atom collisions, the NSSL naturally leads to the notion of dynamical adiabatic states (DAS) and corresponding dynamical adiabatic potential energy curves (DAPEC) [5,9]. In the dynamical adiabatic approximation, the three principal conceptual problems are resolved:

(i) Boundary conditions. In the standard adiabatic basis, there are some matrix elements of nonadiabatic coupling $W_{ij}(R) = \langle i|\partial/\partial R|j\rangle$ between two quasimolecular states $|i\rangle$ and $|j\rangle$ that have a constant component, that is, in principle, we cannot determine the probability of inelastic transition because of nonvanishing transitions at internuclear distances as $R \to \infty$.

(ii) Rotational transitions are transformed into radial transitions through the component of the angular momentum operator L_3 perpendicular to the scattering plane. In standard adiabatic approach, these transitions were beyond the adiabatic scheme and could only be included by numerical close-coupling calculations.

(iii) Here, the ionization process is described using a basis of the complete discrete orthogonal wave packets, which is

————
[*]tasko@ipb.ac.rs

a much more satisfactory approach. In standard adiabatic approach, the continuum states, which have no direct physical meaning, are employed.

In the quantum description of the motion of the nuclei, all of the above-mentioned problems are resolved within the hyperspherical adiabatic approach proposed by Macek [10] for solving the three-body Coulomb problem. Subsequently, the method has been widely applied to a variety of collision problems, in particular to the $He^{2+}+H$ system [11], which we shall treat as an example in the present work. The relationship between the NSSL and hyperspherical adiabatic approach is discussed in Ref. [12].

The DAS and DAPEC have been studied up till now in some detail only for the one-electron model problem, where the interactions of the electron with the target and the projectile centers are described by the zero-range potentials [13]. In the case of one-electron ion-atom systems with Coulomb interactions, only the limits of united atoms and separated atoms have been considered using the perturbation theory [14]. In the present work, we extend the study of DAPEC to all internuclear separations, discuss some of their general properties, and compare our numerical results with existing asymptotic expressions.

We use atomic units throughout the work except unless explicitly stated.

II. FORMULATION OF THE PROBLEM

We consider a collision system consisting of a single electron and two bare nuclei of charges Z_A and Z_B traveling along the straight-line trajectories. The dynamics of the electron is described by the time-dependent Schrödinger equation

$$\left(-\frac{1}{2}\Delta_r - \frac{Z_A}{|\mathbf{r}+\alpha\mathbf{R}|} - \frac{Z_B}{|\mathbf{r}-\beta\mathbf{R}|} \right)\Psi(\mathbf{r},t) = i\frac{\partial\Psi(\mathbf{r},t)}{\partial t},$$
(1)

where $\mathbf{R} = \mathbf{R}_B - \mathbf{R}_A = (vt,\rho,0)$ is the vector connecting the nuclei A and B, v is the impact velocity, ρ is the impact parameter, and the origin of the reference frame is located on the internuclear axis and defined by parameters α and β ($\mathbf{R}_A = -\alpha\mathbf{R}$, $\mathbf{R_B} = \beta\mathbf{R}$, $\alpha + \beta = 1$). This equation is obtained straightforwardly from the three-body Schrödinger equation as accurate semiclassical asymptote with respect to nuclear motion at impact energy much greater than the ionization potential [15]. If electron binding energy is comparable with impact energy, Eq. (1) is not valid. In this case, the total wave function is superposition of nuclear states in the different adiabatic potentials, and a "time" variable, common to all adiabatic channels, cannot be introduced.

The initial condition for $t \to -\infty$ requires that Ψ takes the form of the initial atomic wavefuntion $\Phi^a_\gamma(\mathbf{r}_j)$ localized at one of the two centers ($j = A, B$) with the Galilean translation factor, which takes into account the motion of the nuclei

$$\lim_{t\to-\infty}\Psi(\mathbf{r},t) = \Phi^a_\gamma(\mathbf{r}_j)\exp\left[i\left(\mathbf{v}_j\cdot\mathbf{r}_j + \tfrac{1}{2}v_j^2 t - E^a_\gamma t\right)\right],$$
(2)

where $\mathbf{r}_j = \mathbf{r} - \mathbf{R}_j$, $\mathbf{v}_j$ is the velocity of the jth nucleus and E^a_γ is the atomic energy level.

We introduce the NSSL by dividing the electronic coordinates (x,y,z) by the internuclear separation $R(t)$ and,

subsequently, make the transformation to the rotating (molecular) coordinate system (q_1,q_2,q_3) with the q_1 axis directed along the internuclear axis:

$$q_1 = \frac{1}{R(t)}[x\cos\varphi(t) + y\sin\varphi(t)],$$
(3)

$$q_2 = \frac{1}{R(t)}[-x\sin\varphi(t) + y\cos\varphi(t)],$$
(4)

$$q_3 = \frac{z}{R(t)},$$
(5)

where $\varphi(t) = \arctan(\rho/vt)$ is the polar angle of $\mathbf{R}(t)$ in the scattering (x,y) plane. We also represent the wavefunction in the form

$$\Psi(\mathbf{r},t) = R^{-3/2}\exp\left[i\frac{r^2}{2R}\frac{dR}{dt}\right]f(\mathbf{q},\tau),$$
(6)

where a new time-like variable has been introduced ($\omega = \rho v$):

$$\tau(t) = \int_0^t \frac{dt'}{R^2(t')} = \omega\arctan(vt/\rho),$$
(7)

and the variation of t in the interval $(-\infty, +\infty)$ corresponds to the variation of τ in the interval $(\tau_i,\tau_f) \equiv (-\pi/(2\omega), +\pi/(2\omega))$. The factor $R^{-3/2}$ in Eq. (6) ensures normalization, and the exponent is a generalized translation factor, because it satisfies the relation

$$\exp\left[i\frac{r^2}{2R}\frac{dR}{dt}\right] = \exp\left[i\frac{|\mathbf{r}_j+\mathbf{R}_j|^2}{2R}\frac{dR}{dt}\right]$$
$$= \exp\left[i\left(\mathbf{v}_j\cdot\mathbf{r}_j + \frac{1}{2}v_j^2 t\right)\right]\Bigg|_{Rr_j^{-1}\to\infty}. \quad (8)$$

Substituting the wavefunction Eq. (6) into Eq. (1), we obtain the modified Schrödinger equation

$$H(\tau)f(\mathbf{q},\tau) = i\frac{\partial f(\mathbf{q},\tau)}{\partial\tau},$$
(9)

with

$$H(\tau) = -\frac{1}{2}\Delta_q - R(\tau)\left(\frac{Z_A}{|\mathbf{q}+\alpha\hat{\mathbf{q}}_1|} + \frac{Z_B}{|\mathbf{q}-\beta\hat{\mathbf{q}}_1|}\right)$$
$$+ \omega L_3 + \frac{1}{2}\omega^2 q^2,$$
(10)

where, $R(\tau) = \rho/\cos\omega\tau$, $\hat{\mathbf{q}}_1$ is the unit vector along q_1 axis, and

$$L_3 = -i\left(q_1\frac{\partial}{\partial q_2} - q_2\frac{\partial}{\partial q_1}\right)$$
(11)

is the operator of the projection of the electronic angular momentum onto the direction perpendicular to the scattering plane. In the new $(\mathbf{q},\tau)$ "representation," the two Coulomb centers are at "rest" and separated by the unit distance, but their strengths are $R(\tau)$-dependent.

In the general case of arbitrary trajectories, the last two terms in Hamiltonian Eq. (10) take the form: $R^2\dot{\varphi}(t)L_3 + R^3\ddot{R}q^2/2$ (where the dot represents the derivative with respect to t). Factor $R^2\dot{\varphi}(t)$ coincides (up to the reduced mass of nuclei M) with nuclear angular momentum and is equal ω. For Coulomb trajectory, the strength of oscillator is $R^3\ddot{R} = \omega^2 + Z_A Z_B M^{-1}R$. Since $M^{-1} \sim 10^{-3}$, contribution from the second term is negligible at finite distances R, where inelastic transitions occur.

The Hamiltonian $H(\tau)$ is an even function of τ and the parity $\Pi_3(q_3 \rightarrow -q_3)$ is the only conserved symmetry. We note that the position of the coordinate origin, defined by fixing parameters α and $\beta = 1 - \alpha$, can be taken at will, because the two solutions differing by the shift of the origin along the internuclear axis are related to each other by an unessential coordinate-dependent phase factor [13].

For slow collisions, when an adiabatic approach is appropriate, we look for the solutions of Eq. (9) in the form of an expansion:

$$f(\mathbf{q},\tau) = \sum_\gamma g_\gamma(\tau) \Phi_\gamma(\mathbf{q},\tau) \exp\left[-i \int_0^\tau E_\gamma(\tau') d\tau'\right], \quad (12)$$

in terms of the eigenfunctions $\Phi_\gamma(\mathbf{q},\tau)$ of the instantaneous Hamiltonian Eq. (10):

$$H(\tau) \Phi_\gamma(\mathbf{q},\tau) = E_\gamma(\tau) \Phi_\gamma(\mathbf{q},\tau). \quad (13)$$

We call the complete set of eigenfunctions $\Phi_\gamma(\mathbf{q},\tau)$ DAS and the eigenvalues $E_\gamma(\tau)$ DAPEC, because in addition to internuclear separation $R(\tau)$ they also depend on $\omega = \rho v$. For $\omega \neq 0$, due to the presence of the harmonic oscillator potential in Eq. (10), the spectrum of the Hamiltonian $H(\tau)$ is discrete. One can distinguish two types of DAS that differ by their behavior when $R(\tau) \rightarrow \infty$ [13]. The first type is characterized in this limit by negative eigenvalues and states strongly localized in the vicinity of either of the Coulomb centers Z_A or Z_B. These eigenstates Φ_γ asymptotically correlate with bound (atomic) states Φ_γ^a from Eq. (2). The second type of DAS is characterized in this limit by positive eigenvalues and delocalized eigenfunctions that eventually decay in the classically forbidden region of the harmonic oscillator potential from Eq. (10). They provide a much more adequate description of the ionization channel in terms of a discrete complete set, which transforms back in the original $\mathbf{r}$-space into a set of orthogonal wave packets of free electrons [13]. In the present work, we shall consider only DAPEC of the first type.

After the substitution of Eq. (12) into Eq. (9), the usual set of coupled equations for the expansion coefficients is obtained:

$$\frac{dg_\gamma(\tau)}{d\tau} = -\sum_{\gamma' \neq \gamma} W_{\gamma'\gamma}(\tau) g_{\gamma'}(\tau) \exp\left[i \int_0^\tau \Delta E_{\gamma'\gamma}(\tau') d\tau'\right], \quad (14)$$

where

$$\Delta E_{\gamma'\gamma}(\tau) = E_\gamma(\tau) - E_{\gamma'}(\tau), \quad (15)$$

$$W_{\gamma'\gamma}(\tau) = \langle \Phi_{\gamma'} | \frac{\partial}{\partial\tau} | \Phi_\gamma \rangle. \quad (16)$$

If initially the electron is bound in the atomic state $\Phi_{\gamma_i}^a$, then the set of coupled Eqs. (14) has to be solved with initial conditions

$$g_\gamma(\tau_i) = \delta_{\gamma,\gamma_i}, \quad (17)$$

and the transition probability to final state γ_f is given by

$$P(\rho,v) = |g_{\gamma_f}(\tau_f)|^2. \quad (18)$$

The label γ_f can correspond to a bound state on the same center as γ_i, in which case we deal with the excitation process, or to a bound state on the other center when we deal with charge

exchange, or it can correspond to delocalized ("continuum") state when we deal with ionization. Note also that, because the parity Π_3 is conserved, the symmetric and antisymmetric components of the initial state evolve independently.

In the case of the homonuclear system, $Z_A = Z_B$, there is additional (gerade-ungerade) symmetry related to the parity $\Pi(\mathbf{q} \rightarrow -\mathbf{q})$, and the definitions of initial conditions and transition probabilities have to be modified accordingly [13].

III. METHOD OF CALCULATION

The Hamiltonian Eq. (10) is formally similar to the Hamiltonian describing the one-electron diatomic ion in an external magnetic field. The calculation of the spectrum of the latter (in the case of H_2^+ ion) has recently been performed [16,17] by using the Lagrange-mesh method [18]. In order to solve the eigenvalue Eq. (13), we shall therefore closely follow the method of Refs. [16,17]. Choosing for convenience the coordinate origin at the midpoint of the internuclear separation, $\alpha = \beta = 1/2$, we introduce the prolate spheroidal coordinates:

$$\xi = |\mathbf{q} + \tfrac{1}{2}\hat{\mathbf{q}}_1| + |\mathbf{q} - \tfrac{1}{2}\hat{\mathbf{q}}_1| - 1, \quad (19)$$

$$\eta = |\mathbf{q} + \tfrac{1}{2}\hat{\mathbf{q}}_1| - |\mathbf{q} - \tfrac{1}{2}\hat{\mathbf{q}}_1|, \quad (20)$$

$$\phi = \arctan(q_3/q_2). \quad (21)$$

The coordinate ξ is shifted with respect to traditional definition in order to make its definition interval $[0,\infty)$. The range of η is $[-1,1]$ and that of ϕ is $[0,2\pi)$. The volume element is

$$dV = \tfrac{1}{8} J(\xi,\eta) d\xi d\eta d\phi, \quad (22)$$

$$J(\xi,\eta) = (\xi + 1)^2 - \eta^2. \quad (23)$$

In these coordinates, the Hamiltonian Eq. (10) reads

$$H = T + V + \omega L_3, \quad (24)$$

where the kinetic energy operator is

$$T = \frac{2}{J(\xi,\eta)}(T_\xi + T_\eta) - \frac{2}{\xi(\xi+2)(1-\eta^2)}\frac{\partial^2}{\partial\phi^2}, \quad (25)$$

$$T_\xi = -\frac{\partial}{\partial\xi}\xi(\xi+2)\frac{\partial}{\partial\xi}, \quad (26)$$

$$T_\eta = -\frac{\partial}{\partial\eta}(1-\eta^2)\frac{\partial}{\partial\eta}, \quad (27)$$

the potential is the sum of Coulomb interactions and the oscillator term

$$V = -\frac{2R}{J(\xi,\eta)}[(Z_A + Z_B)(\xi+1) + (Z_B - Z_A)\eta]$$
$$+ \frac{1}{8}\omega^2[(\xi+1)^2 + \eta^2 - 1], \quad (28)$$

and the angular momentum operator is given by

$$L_3 = -\frac{i}{J(\xi,\eta)}\Big[\eta\sqrt{1-\eta^2}L_{3\xi} - (\xi+1)\sqrt{\xi(\xi+2)}L_{3\eta}\Big]\cos\phi$$
$$+ i\frac{(\xi+1)\eta}{\sqrt{\xi(\xi+2)(1-\eta^2)}}\sin\phi\frac{\partial}{\partial\phi}, \quad (29)$$

$$L_{3\xi} = \sqrt{\xi(\xi+2)}\frac{\partial}{\partial\xi}, \quad (30)$$

$$L_{3\eta} = \sqrt{1-\eta^2}\frac{\partial}{\partial\eta}. \quad (31)$$

Next, we define a set of $N_\xi N_\eta$ mash points ($\xi_i = hx_i, \eta_j$)($i = 1, \ldots, N_\xi, j = 1, \ldots, N_\eta$), related to zeros of the Laguerre and Legendre polynomials [19]: $L_{N_\xi}(x_i) = 0$ and $P_{N_\eta}(\eta_j) = 0$. The dimensionless parameter h allows for the scaling of the mash along the ξ coordinate. With each of these one-dimensional mashes, we can associate the corresponding approximate Gaussian quadrature formulas [19]. With the help of these mashes, we define the three-dimensional basis functions:

$$F_{ijm}^{\pi_3}(\xi,\eta,\phi) = \left(\frac{8}{J_{ij}}\right)^{1/2} f_i^\nu(\xi) g_j^\nu(\eta) h_m^{\pi_3}(\phi), \qquad (32)$$

where

$$J_{ij} = (hx_i + 1)^2 - \eta_j^2. \qquad (33)$$

The azimuthal-angle-dependent basis functions $h_m^{\pi_3}(\phi)$, which are eigenfunctions both of $\Pi_3(q_3 \to -q_3) \equiv \Pi_3(\phi \to 2\pi - \phi)$ and of $L_1^2 = -\partial^2/\partial\phi^2$ corresponding to eigenvalues $\pi_3 = \pm 1$ and m^2, with $m = |m_1| = 0,1,\ldots,M$, are defined as

$$h_m^{\pi_3}(\phi) = \begin{cases} [(1+\delta_{m,0})\pi]^{-1/2} \cos m\phi & \text{for} \quad \pi_3 = 1 \\ (\pi)^{-1/2} \sin m\phi & \text{for} \quad \pi_3 = -1. \end{cases} \qquad (34)$$

The regularized Lagrange-Laguerre functions [16,17] are defined as

$$f_i^\nu(\xi) = (-1)^i (hx_i)^{1/2} \left(\frac{\xi(\xi+2)}{hx_i(hx_i+2)}\right)^{\nu/2} \frac{L_{N_\xi}(\xi/h)}{\xi - hx_i} e^{-\xi/2h}, \qquad (35)$$

and the regularized Lagrange-Legendre functions as

$$g_j^\nu(\eta) = (-1)^{N_\eta - j} \sqrt{\frac{1-\eta_j^2}{2}} \left(\frac{1-\eta^2}{1-\eta_j^2}\right)^{\nu/2} \frac{P_{N_\eta}(\eta)}{\eta - \eta_j}, \qquad (36)$$

where the "regularization parameter" ν corrects the behavior of the Lagrange functions at $\xi = 0$, $\eta = \pm 1$ and handles the singularity in the second term of Eq. (25). Thus, we take $\nu = 0$ for m even and $\nu = 1$ for m odd [16,17].

The matrix elements of the Hamiltonian Eq. (24) in the basis Eq. (32) are calculated by using Gaussian quadratures for integrals over ξ and η and analytical integration over ϕ. The basis Eq. (32) is orthonormal when overlaps are calculated in this way. The technical details of calculation can be found in Refs. [16,17], so that we only give in the Appendix the final explicit expressions for all matrix elements.

IV. RESULTS AND DISCUSSION

Once we have the matrix representation of the Hamiltonian, the eigenvalue problem Eq. (13) can be solved by numerical diagonalization. We shall present here the results for $Z_A = 1$ and $Z_B = 2$, that is for (HeH)$^{2+}$ quasimolecular system. The matrix representation given in the Appendix separates blocks with different $\pi_3 = \pm 1$ symmetries.

The solid (black) curves in Fig. 1 show the R-dependence of the 90 lowest symmetric ($\pi_3 = 1$) eigenvalues $E(R,\omega)$ for $\omega = 1$. These results and others shown in this section (except when it is explicitly indicated) have been obtained using the basis with $(N_\xi, N_\eta, M) = (20,10,9)$ and $h = 0.2$. As a dominant structure, one can notice the four overlapping
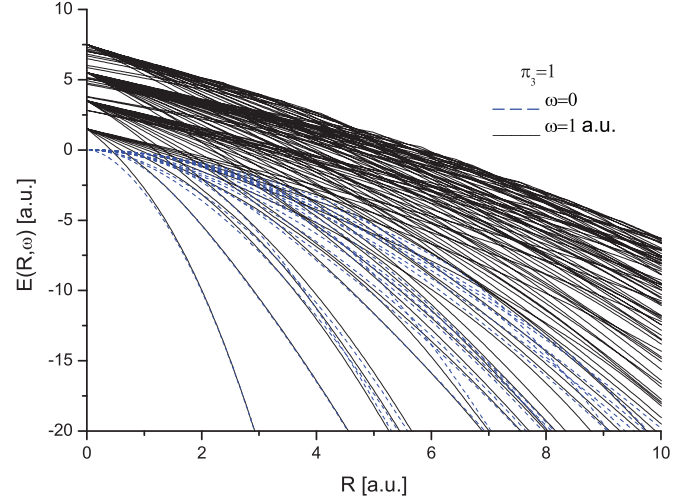

FIG. 1. (Color online) The 90 lowest eigenvalues (DAPEC and "ghosts") for symmetric ($\pi_3 = 1$) states of the (HeH)$^{2+}$ collision system ($Z_A = 1, Z_B = 2$) as functions of the internuclear separation R for $\omega = 1$ a.u. [solid (black) curves] and the lowest 20 DAPEC for $\omega = 0$ [dashed (blue) curves].

manifolds of DAPEC, which start at $R = 0$ from the points of high degeneracy corresponding to oscillator-like energies:

$$E(0,\omega) = (N + 3/2)\omega, \quad N = 0,2,4,6,\ldots \qquad (37)$$

and then spreading toward larger distances where they all tend toward large negative values. Actually, the eigenvalues at $R = 0$ given by Eq. (37) are infinite-fold degenerate. This can be proved by application of the perturbation theory, as will be shown in the next subsection. At any finite value of R, the degeneracy is excluded by the Neumann-Wigner theorem [20], which forbids the exact crossing of two DAPEC of the same symmetry.

The dashed (blue) curves in Fig. 1 are the 20 lowest symmetric DAPEC for $\omega = 0$. As can be seen from Eq. (10) in the case $\omega = 0$, DAPEC are related to the usual PEC $\varepsilon(R)$ of the (HeH)$^{2+}$ molecular ion by relation

$$E(R,0) = \varepsilon(R)R^2. \qquad (38)$$

One can notice that the dashed (blue) and solid (black) curves merge as $R \to \infty$.

Besides this dominant DAPEC structure, there are some additional eigenvalues that deviate from the described behavior, as is clearly seen at small internuclear separations. We call these the "ghost eigenvalues," and their origin and behavior is discussed in more details in the next subsection.

Similar dominant structure of DAPEC and existence of ghost eigenvalues is also found for antisymmetric ($\pi_3 = -1$) states. The only difference is that degenerate manifolds at $R = 0$, which are again given by Eq. (37), now correspond to $N = 1,3,5,7,\ldots.$

A. Small internuclear separations

The region of small internuclear separations is shown with larger resolution in Fig. 2 for symmetric states. The appearance of ghost eigenvalues are clearly seen here.
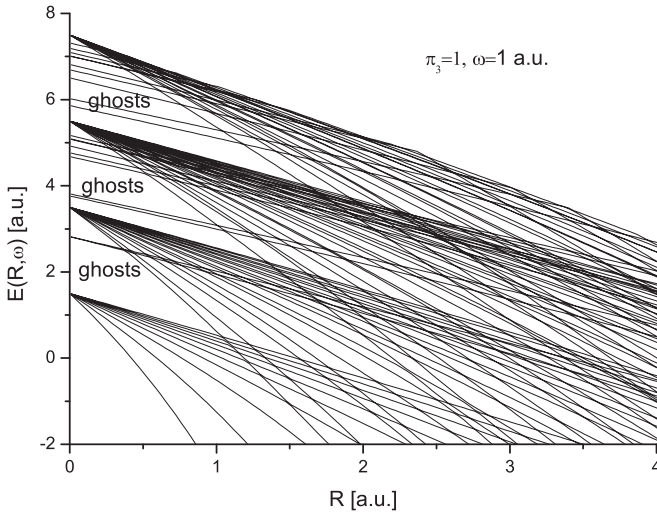
FIG. 2. Magnification of the region of small internuclear separations from Fig. 1. Spurious eigenvalues are labeled as "ghosts."

1. Perturbation theory

The dominant structure of DAPEC manifolds emerging from the oscillator levels in the united-atom limit $R \to 0$ has been predicted and explained by the first-order perturbation theory [14]. In this approach, the Coulomb interaction (proportional to R) has been treated as a perturbation of the zero-order Hamiltonian given by the sum of the oscillator and angular momentum terms in Eq. (10). With additional assumption of small $\omega \ll 1$ particularly simple expression holds:

$$E_{klm_3}(R,\omega) \approx (2k + l + m_3 + 3/2)\omega - I_{kl}(Z_A + Z_B)R\omega^{1/2}, \quad (39)$$

where, $k = 0, 1, \ldots$ is the radial quantum number, $l = 0, 1, \ldots$ and $m_3 = -l, \ldots, l$ are angular momentum quantum numbers of the three-dimensional spherical harmonic oscillator and I_{kl} are coefficients expressed in terms of some simple integrals [14]. Comparing with Eq. (37), we have $N = 2k + l + m_3$ and $\pi_3 = (-1)^{l+m_3} = (-1)^N$.

For the first few symmetric and antisymmetric manifolds, the coefficients I_{kl} are given by simple analytic expressions [14]. For example, in the case of the first symmetric manifold, we have: $N = 0, k = 0, m_3 = -l, l = 0, 1, \ldots$, and

$$E_{0l-l}(R,\omega) \approx \frac{3}{2}\omega - \frac{\Gamma(l+1)}{\Gamma(l+3/2)}(Z_A + Z_B)R\omega^{1/2}, \quad (40)$$

where $\Gamma(z)$ is the Γ function. These perturbational estimates are compared in Fig. 3 [dashed (red) lines] with the numerical results [solid (black) lines]. One can see that agreement is satisfactory even though we consider the case $\omega = 1$ and the estimate Eq. (40) has been derived assuming that ω is small. Also shown in Fig. 3 is the limiting line corresponding to the case $l \to \infty$ in Eq. (40), indicating that there is an infinite number of DAPEC in the manifold. The higher manifolds ($N \geqslant 2$) can contain more than one series of DAPEC of the form of Eq. (39). For example, in the $N = 2$ case we have two series: $\{k = 1, l, m = -l\}, l = 0, 1, \ldots$ and $\{k = 0, l, m = -l + 2\}, l = 1, 2, \ldots$ [14].
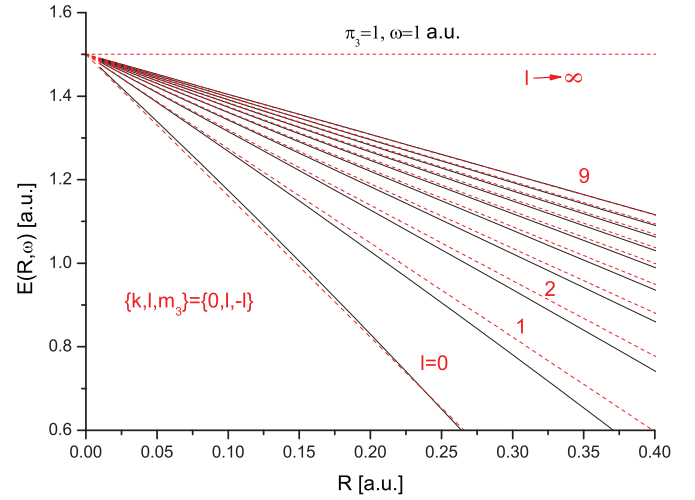

FIG. 3. (Color online) The lowest ($N = 0$) manifold from Fig. 2 at very small internuclear separations [solid (black) lines] together with the predictions of the perturbation theory Eq. (40) [dashed (red) lines].

2. Ghost eigenvalues

"Ghost eigenvalues" have been reported before, when using the Lagrange-mash-related methods such as discrete variable representation (DVR) [21] or Fourier grids [22]. In Ref. [21], the origin of these spurious eigenvalues has been attributed to the fact that matrix elements are calculated using the quadrature approximations. This procedure generates first-order perturbation theory corrections to the variational eigenvalues (obtained with numerically exact matrix elements), as opposed to second-order corrections due to the truncation of the variational bases. The appearance of the nonphysical eigenvalues has been also reported when using Lagrange-mash method in the problem of the H_2^+ in the external magnetic field [16,17]. There, it has also been attributed to the use of the Gaussian quadratures but no explanations were given.

In our opinion, the appearance of ghost eigenvalues in our case is not due to the use of Gaussian quadrature but rather to the special structure of the spectrum at $R \to 0$, namely the infinite order of degeneracy of all eigenvalues in this limit. As can be seen from Eq. (39), the small values of N can be achieved by highly excited (large $2k + l$) oscillator states and extremal (large negative m_3) angular momentum states, which correspond to the edge of the employed basis. In any finite basis (including ours) these states may have bad (incorrect) representation and, therefore, lead to the appearance of ghost eigenvalues in our calculation.

Table I shows the eigenvalues $E(R,\omega)$ at $R = 0.01$ and mean values $\langle L_3 \rangle$ for the first 12 symmetric eigenstates in the cases of $\omega = 1$ and $\omega = 0.2$. The basis used in the calculation is defined by $(N_\xi, N_\eta, M) = (20, 10, 9)$ with scaling parameter $h = 0.2$ (in the case $\omega = 1$) and $h = 1$ (in the case $\omega = 0.2$). The first 10 DAS correspond to DAPEC shown in Fig. 3 and are labeled by the quantum number $m_3 = -l$ ($l = 0, 1, \ldots 9$). One can see that $\langle L_3 \rangle \approx m_3$ for the first 10 DAS and this relation is better fulfilled in the $\omega = 0.2$ case, in accord with the above-mentioned perturbation theory. The last two states labeled as "ghosts" in Table I correspond to the first almost

TABLE I. Calculated eigenvalues $E(R,\omega)$ and mean values $\langle L_3 \rangle$ for the first 12 symmetric eigenstates at $R = 0.01$, in the cases of $\omega = 1$ and $\omega = 0.2$. The label m_3 is defined in Eq. (39) and in Fig. 3. The basis used is defined by $(N_\xi, N_\eta, M) = (20,10,9)$ with scaling parameter $h = 0.2$ (for $\omega = 1$) and $h = 1$ (for $\omega = 0.2$). All quantities are in atomic units.

m_3	$R = 0.01, \omega = 1$		$R = 0.01, \omega = 0.2$	
	$E(R,\omega)$	$\langle L_3 \rangle$	$E(R,\omega)$	$\langle L_3 \rangle$
0	1.4683	−0.055	0.28495	−0.006
−1	1.4771	−1.017	0.28983	−1.005
−2	1.4817	−2.029	0.29189	−2.006
−3	1.4843	−3.028	0.29305	−3.006
−4	1.4861	−4.028	0.29383	−4.006
−5	1.4874	−5.027	0.29439	−5.005
−6	1.4884	−6.015	0.29483	−6.005
−7	1.4892	−6.963	0.29517	−7.005
−8	1.4899	−7.995	0.29546	−8.003
−9	1.4906	−8.846	0.29571	−8.953
Ghost	2.8112	−11.161	0.55938	−11.102
Ghost	2.8126	−12.163	0.55965	−12.089

degenerate pair of ghost levels shown in Fig. 2. It is apparent that the values of $\langle L_3 \rangle$ for the ghost states are out of the range $(|\langle L_3 \rangle| \leqslant 9)$, where the correct representation can be expected within the employed basis ($N_\eta = 10, M = 9$).

Using spherical coordinates $\{q, \theta_3 = \arccos(q_3/q), \phi_3 = \arctan(q_2/q_1)\}$, we show in Fig. 4(a) (the case $\omega = 1$) and in Fig. 4(b) (the case $\omega = 0.2$) moduli $|\Phi_\gamma(q,\theta_3,\phi_3; R)|$ of the first 12 eigenfunctions as functions of ϕ_3 at the fixed values of $q = 2, \theta_3 = \pi/4$ and for $R = 0.01$. One can see that in both cases the first 10 DAS show smooth dependence on ϕ_3, while the ghost states exhibit irregular oscillatory behavior. In addition, again in accord with the perturbation theory, it is obvious that the 10 DAS are in the case $\omega = 0.2$ closer to unperturbed eigenfunctions of L_3 (which would be represented as constants). Only the interval $(0, \pi)$ for the argument ϕ_3 is shown in Fig. 4, because the eigenfunctions
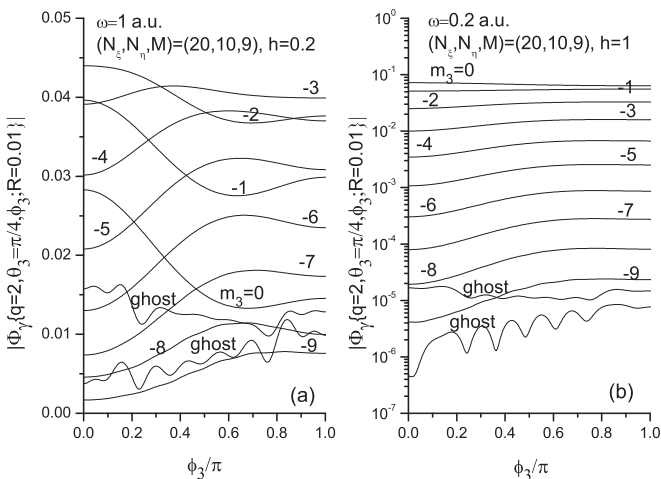
have the property $\Phi_\gamma(q,\theta_3,\phi_3; R) = \Phi^*_\gamma(q,\theta_3, 2\pi - \phi_3; R)$. This property follows from the fact that the transformation $\phi_3 \to 2\pi - \phi_3$ in the Hamiltonian Eq. (10) only changes the sign of the operator L_3.

The ghost eigenvalues are sensitive to the basis size. When the basis size is increased, the number of converged DAPEC in physical manifolds increases, while the positions and number of ghost eigenvalues in a given energy range are changed.

It is important to establish if ghost eigenvalues affect the physical DAPEC through the series of avoided crossings, which on the scale of Fig. 2 appear as exact crossings. We have indeed verified that the widths of these avoided crossings are practically negligible ($< 10^{-10}$ a.u.), so that they should not affect physical processes. In addition, the slope of the ghost eigenvalues is smaller than that of the shown physical DAPEC, and at larger internuclear separations R, the former are eventually shifted toward the highly excited (and probably not converged) levels. Therefore, the existence of the ghost eigenvalues at intermediate and large separations can be ignored.

B. Intermediate and large internuclear separations

Due to the relationship Eq. (38) between the DAPEC and the ordinary PEC, it is more convenient to consider the case of intermediate and especially large internuclear separations by studying the R-dependence of the scaled DAPEC: $E(R,\omega)/R^2$. Figure 5 shows the DAPEC from Fig. 1 in this new representation. In the case of $\omega = 1$, the four overlapping manifolds are still visible at small internuclear separations, but the scaled DAPEC diverge in this region. In addition, here it is clearly seen how DAPEC and PEC merge together at large internuclear separations. In all calculations with $\omega = 0$, in order to obtain the correct behavior of PEC in the united-atom ($R \to 0$) and separated-atoms ($R \to \infty$) limits, the scaling factor h for the ξ coordinate in Eq. (35) has been taken in the form

$$h = \frac{2}{(Z_A + Z_B)R}. \tag{41}$$

In Figs. 6 and 7, the fragment of low-lying, respectively, symmetric and antisymmetric DAPEC are shown [solid (black)

FIG. 4. Moduli $|\Phi_\gamma(q,\theta_3,\phi_3; R)|$ of the first 12 eigenfunctions as functions of ϕ_3 at the fixed values of $q = 2, \theta_3 = \pi/4$, $R = 0.01$ for (a) $\omega = 1$ and (b) $\omega = 0.2$. Spurious eigenstates are labeled as "ghosts."
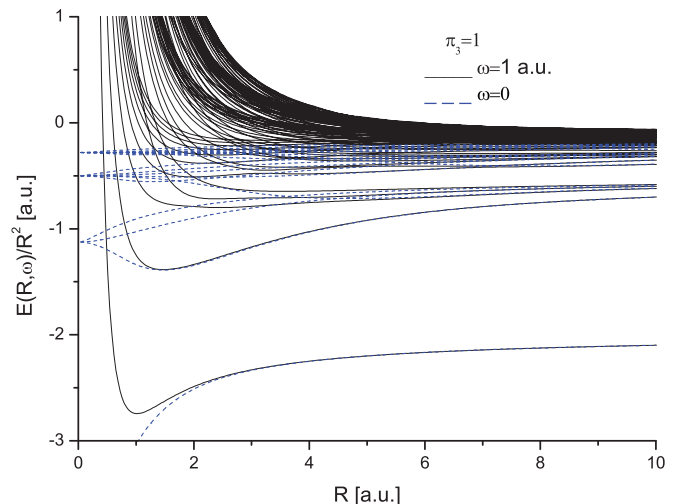

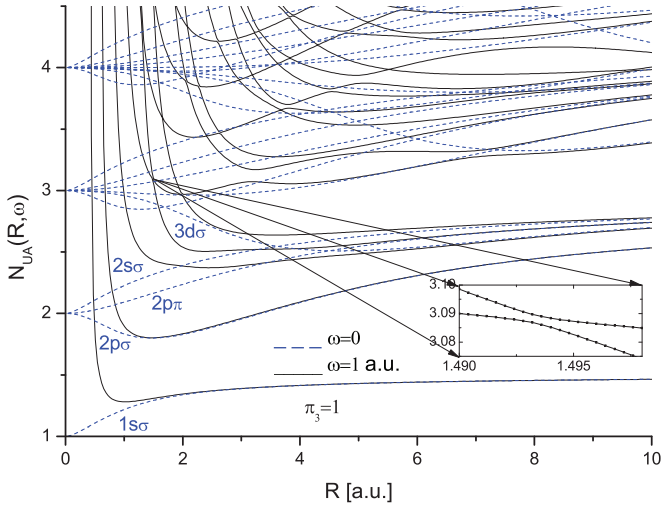FIG. 5. (Color online) Scaled (divided by R^2) DAPEC from Fig. 1.

FIG. 6. (Color online) Segment of low-lying scaled DAPEC from Fig. 5 represented in terms of "effective united atom principal quantum number" Eq. (42) [solid (black) curves]. Also shown [dashed (blue) curves] are the standard PEC of the $(HeH)^{2+}$ molecular ion labeled by united-atom quantum numbers. The inset shows enlarged region of the avoided crossing between two DAPEC located around $(R = 1.493, N_{UA} = 3.088)$.

curves] together with the ordinary PEC [dashed (blue) curves]. Instead of the eigenvalues, however, for better representation of the excited states, we show the "effective united atom principal quantum number" as a function of R:

$$N_{UA}(R,\omega) = (Z_A + Z_B)R[-2E(R,\omega)]^{-1/2}. \qquad (42)$$

Both sets of curves, corresponding to DAPEC and PEC, asymptotically (as $R \to \infty$) approach unperturbed atomic levels, although there are some differences in asymptotic behavior, which are not visible in these figures but will be discussed in the next subsection. In any case, this representation is useful in predicting which DAPEC are important to be included when describing various inelastic processes. DAPEC are characterized by a large number of avoided crossings,
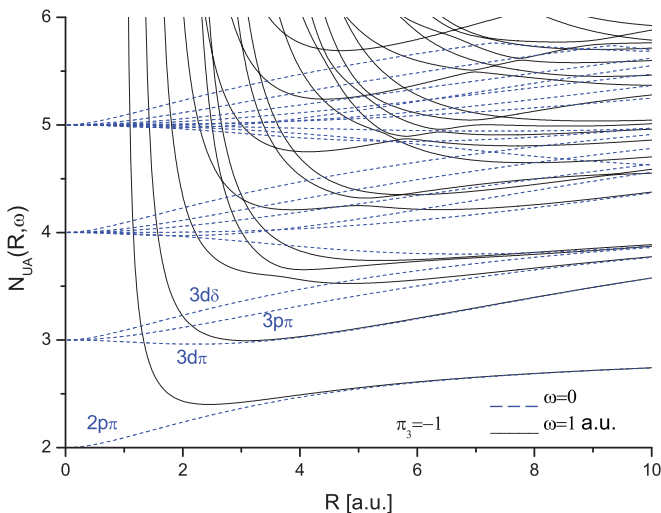

FIG. 7. (Color online) Same as described in the legend of Fig. 6 but for antisymmetric ($\pi_3 = -1$) states.

which indicate the regions of strong couplings and localized transitions. The effect of rotation of the internuclear axis is already incorporated in DAPEC, and all couplings are of "radial" type. Thus, for example, the exact crossing in Fig. 6 between the $3d\sigma$ and $2p\pi$ PEC, which in standard adiabatic representation indicates a region of strong rotational coupling, appears as an avoided crossing between two DAPEC.

At first sight, it looks like there are many exact crossings of DAPEC in Fig. 6. However, this is a wrong impression due to the given scale. On a more finer scale these crossings appear as a very narrow avoided crossings (see the insert in Fig. 6). The exact crossings are forbidden since we are dealing with a 3D nonseparable problem [20]. On the other hand, the existence of narrow avoided crossings indicates that our system is close to some separable system.

The hidden-crossings are not visible in Figs. 6 and 7. They should appear at the internuclear distances when the eigenenergy $E_n(R)$ touches the top of effective potential determining electron motion. Such a mechanism was demonstrated in hyperspherical adiabatic representation at zeroth total angular momentum for positronium (see Figs. 1 and 3 in Ref. [23]) and helium atom (see Fig. 13 in Ref. [24]). But in the dynamical adiabatic representation, the effective potential cannot be presented in standard form due to the *differential* operator ωL_3. This operator, together with parabolic potential $\omega q^2/2$, has a meaning similar to a uniform magnetic field and is translational covariant (like a constant); i.e., the Schrödinger equation obeys gauge invariance with respect to a shift of the reference frame along the internuclear axis and the wave function acquires a phase factor.

1. Asymptotic behavior

The limit of separated atoms ($R \to \infty$) has been studied in Ref. [14] by applying perturbation theory. The result obtained for the asymptotic behavior of a DAPEC $E_{nsr}(R,\omega)$, which tends asymptotically toward a bound state on center Z_A can conveniently be represented in the form

$$\Delta E_{nsr}(R,\omega) \equiv E_{nsr}(R,\omega) + \frac{Z_A^2}{2n^2}R^2 + Z_B R$$

$$= C_0(\omega) + \frac{C_1(\omega)}{R} + O\left(\frac{1}{R^2}\right), \qquad (43)$$

$$C_0(\omega) = s\left[\omega^2 + \left(\frac{3nZ_B}{2Z_A}\right)^2\right]^{1/2}, \qquad (44)$$

$$C_1(\omega) = -\frac{Z_B n^2}{4Z_A^2 R}\left[-2n^2 + 2 + 12s^2 + \frac{3\omega^2}{\omega^2 + \left(\frac{3nZ_b}{2Z_A}\right)^2}\right.$$

$$\left. \times \left(n^2 - 1 - 4s^2 - 2\lambda_r^{ns}\right)\right], \qquad (45)$$

where n is the atomic principal quantum number, $s = 0, \pm 1, \ldots, \pm (n-1)$ is the Stark quantum number, λ_r^{ns} ($r = 0, 1, \ldots, n - |s| - 1$) with the convention $\lambda_0^{ns} < \lambda_1^{ns} < \cdots < \lambda_{n-|s|-1}^{ns}$ are the eigenvalues of a simple tridiagonal matrix [14] and parity $\pi_3 = (-1)^r$.

For heteronuclear systems, another series of levels for states localized on center Z_B are obtained from Eq. (43) by the interchange $Z_A \leftrightarrow Z_B$ and $(n,s,r) \to (n',s',r')$. Note that by letting $\omega = 0$, Eq. (43) gives the first four terms
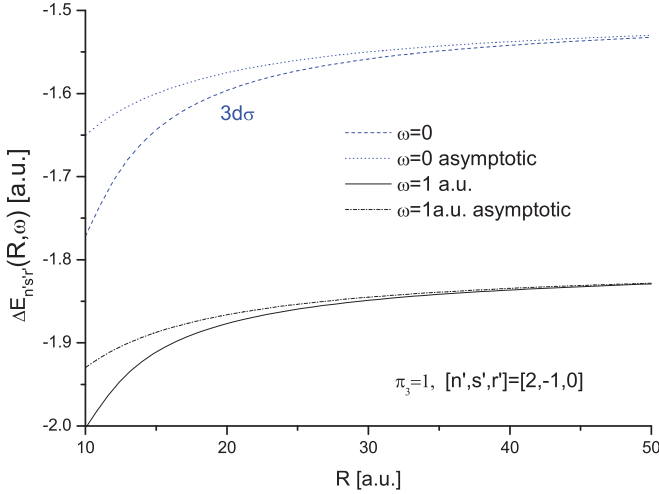
FIG. 8. (Color online) Numerically calculated expression $\Delta E(R,\omega) = E(R,\omega) + (1/2)R^2 + 1/R$ for the DAPEC corresponding to $\omega = 1$ [solid (black) curves], which approaches the asymptote [dashed-dotted (black) curve] given by Eq. (46). Dashed (blue) curve corresponds to the $\omega = 0$ case and doted (blue) curve to the asymptote given by Eq. (47).

of the asymptotic expansion of the ordinary PEC, $\varepsilon(R) = E(R,0)/R^2$ of the two-Coulomb-center problem.

We illustrate the correct asymptotic behavior of numerically calculated DAMPEC in our case of $Z_A = 1$, $Z_B = 2$ and $\omega = 1$ by considering the particular level from $n' = 2$ manifold labeled by quantum numbers $[n',s',r'] = [2, -1, 0]$, which according to Eq. (43) and $\lambda_0^{2-1} = 0$ [14] approaches the asymptote:

$$\Delta E_{2-10}(R;\omega = 1) \approx -\frac{\sqrt{13}}{2} - \frac{33}{26R}. \quad (46)$$

In Fig. 8 we show results of numerical calculations [solid (black) line] and demonstrate that, at large separations, they approach the asymptotic result Eq. (46) [dashed-dotted (black) line]. In order to treat these large separations correctly, it was necessary to increase the number of η-grid points to $N_\eta = 25$ and to use the scaling of the ξ coordinate from Eq. (41), while keeping $N_\xi = 20$. Sufficient accuracy (for the scale of Fig. 8) was obtained with $M = 5$. The analogous dashed (blue) curve in Fig. 8 corresponds to $\omega = 0$, in which case the asymptote,

$$\Delta E_{2-10}(R;\omega = 0) \approx -\frac{3}{2} - \frac{3}{2R}, \quad (47)$$

is represented by dashed-double-dotted (blue) line. From Fig. 8, we can see the difference in asymptotic behavior of DAPEC and PEC, which is difficult to detect in Figs. 5, 6, and 7.

If one is interested in estimates of internuclear distances at which DAPEC corresponding to $\omega \neq 0$ merge with those with $\omega = 0$ (as in Fig. 1 and Figs. 5–7), these can be determined by considering the relative deviations

$$\delta_{nsr}(R;\omega) = \left| \frac{E_{nsr}(R,\omega) - E_{nsr}(R,0)}{E_{nsr}(R,\omega)} \right| \quad (48)$$

and determining R from the above equation by requiring that, for example, $\delta_{nsr}(R;\omega) = 1\%$. By using asymptotic expansions (43)–(45), Eq. (48) is converted to algebraic equation of third degree for determining R:

$$\delta_{nsr}(R;\omega) = \left| \frac{[C_0(\omega) - C_0(0)]R + C_1(\omega) - C_1(0)}{-\frac{Z_A^2}{2n^2}R^3 - Z_B R^2 + C_0(\omega)R + C_1(\omega)} \right|. \quad (49)$$

Thus, in the case of the above considered example of the state asymptotically localized on center $Z_B = 2$ with quantum numbers $[n', s', r'] = [2, -1, 0]$, we find that $\delta_{2-10} = 1\%$ for $R = 6.06$ while $\delta_{2-10} = 0.5\%$ for $R = 9.42$.

V. CONCLUDING REMARKS

We have studied the global structure of DAPEC for one-electron atomic collision systems by using the example of $(\text{HeH})^{2+}$ collision system for the case of straight-line trajectories of the nuclei and collisions in which the impact parameter and relative collision velocity are related by $\rho v = 1$. The previous analytic predictions concerning the behavior of DAPEC in the united-atom and separated-atom limits, obtained by application of perturbation theory [14], have been quantitatively confirmed by numerically calculated DAPEC. The numerical method, based on the Lagrange meshes, allows for the efficient calculation of DAPEC over a wide range or internuclear separations. At small separations, however, it leads to the appearance of "ghost eigenvalues," which could, in principle, cause problems in further applications of DAPEC. These eigenvalues, however, seem not to interact with the physical DAPEC and are shifted upwards at larger separations, so that they shouldn't affect the description of the dynamics involving only low-lying states, which is the next step in the application of the methods and results presented in this work.

It should be noted that all DAPEC that have been considered in the present work correspond to the type which asymptotically (as $R \to \infty$) correspond to bound states of the electron on either of the nuclei. They are appropriate for describing excitation and charge-exchange processes. The second type of the DAPEC which describe delocalized states relate to the description of the physical continuum states and ionization processes [13], which are out of the scope of the present paper.

APPENDIX: EXPRESSIONS FOR MATRIX ELEMENTS

All matrix elements can be derived in closed form. Although Gaussian quadratures are used when calculating matrix elements, they depend only on the grid points and not on quadrature weights. It turns out that some operators (e.g., T_ξ and L_3) are not represented by Hermitian matrices in the bases

Eq. (32). In these cases, the symmetrization procedure [16,17] is applied, i.e., in order to represent an operator O we take the mean of the matrix element and its Hermitian conjugate:

$$\langle a|\tilde{O}|b\rangle = \tfrac{1}{2}(\langle a|O|b\rangle + \langle b|O|a\rangle^*). \tag{A1}$$

We have actually verified numerically that the non-Hermitian matrix representation of the Hamiltonian Eq. (24) has the same spectrum as the symmetrized form, the latter is simply more convenient for numerical diagonalization.

The matrix elements of the kinetic energy operator Eq. (25) are given by

$$\langle F_{ijm}^{\pi_3}|\tilde{T}|F_{i'j'm'}^{\pi_3}\rangle = 2(J_{ij}J_{i'j'})^{-1/2}(\langle f_i^\nu|\tilde{T}_\xi|f_{i'}^\nu\rangle\delta_{jj'}$$
$$+ \langle g_j^\nu|T_\eta|g_{j'}^\nu\rangle\delta_{ii'})\delta_{mm'}$$
$$+ \frac{2m^2\delta_{ii'}\delta_{jj'}\delta_{mm'}}{hx_i(hx_i+2)(1-\eta_j^2)}, \tag{A2}$$

where for $i \neq i'$

$$\langle f_i^0|T_\xi|f_{i'}^0\rangle = (-1)^{i+i'}\frac{(x_ix_{i'})^{1/2}}{(x_i+x_{i'})^2}\left(x_i+x_{i'}+\frac{4}{h}\right), \tag{A3}$$

$$\langle f_i^1|\tilde{T}_\xi|f_{i'}^1\rangle = \frac{1}{2}\langle f_i^0|T_\xi|f_{i'}^0\rangle\frac{x_i(hx_i+2)+x_{i'}(hx_{i'}+2)}{\sqrt{x_i(hx_i+2)x_{i'}(hx_{i'}+2)}}$$
$$- \frac{(-1)^{i+i'}}{h(x_i-x_{i'})}\left[\sqrt{\frac{x_i(hx_i+2)}{x_{i'}(hx_{i'}+2)}}(hx_i+1)\right.$$
$$\left.- \sqrt{\frac{x_{i'}(hx_{i'}+2)}{x_i(hx_i+2)}}(hx_{i'}+1)\right], \tag{A4}$$

for $i = i'$

$$\langle f_i^0|T_\xi|f_i^0\rangle = -\frac{x_i^2}{12} + \frac{x_i}{6}\left(2N_\xi+1-\frac{1}{h}\right)$$
$$+ \frac{1}{3hxi}[(h+2N_\xi+1)x_i-1], \tag{A5}$$

$$\langle f_i^1|\tilde{T}_\xi|f_i^1\rangle = \langle f_i^0|T_\xi|f_i^0\rangle - \frac{1}{hx_i(hx_i+2)} + \frac{1}{hx_i} - 1, \tag{A6}$$

for $j \neq j'$

$$\langle g_j^0|T_\eta|g_{j'}^0\rangle = 2(-1)^{j+j'}\frac{(1-\eta_j^2)^{1/2}(1-\eta_{j'}^2)^{1/2}}{(\eta_j-\eta_{j'})^2}, \tag{A7}$$

$$\langle g_j^1|T_\eta|g_{j'}^1\rangle = 2(-1)^{j+j'}\frac{(1-\eta_j\eta_{j'})}{(\eta_j-\eta_{j'})^2}, \tag{A8}$$

and for $j = j'$

$$\langle g_j^0|T_\eta|g_j^0\rangle = \frac{N_\eta(N_\eta+1)}{3} - \frac{2}{3(1-\eta_j^2)}, \tag{A9}$$

$$\langle g_j^1|T_\eta|g_j^1\rangle = \langle g_j^0|T_\eta|g_j^0\rangle + \frac{1}{1-\eta_j^2}. \tag{A10}$$

The potential term Eq. (28) is represented simply by diagonal matrix

$$\langle F_{ijm}^{\pi_3}|V|F_{i'j'm'}^{\pi_3}\rangle = -\frac{2R}{J(hx_i,\eta_j)}[(Z_A+Z_B)(hx_i+1)$$
$$+ (Z_B-Z_A)\eta_j]\delta_{ii'}\delta_{jj'}\delta_{mm'}$$
$$+ \frac{1}{8}\omega^2[(hx_i+1)^2+\eta_j^2-1]\delta_{ii'}\delta_{jj'}\delta_{mm'}. \tag{A11}$$

The matrix elements of the L_3 operator Eq. (29) are given by

$$\langle F_{ijm}^{\pi_3}|\tilde{L}_3|F_{i'j'm'}^{\pi_3}\rangle = -\frac{i}{2}(J_{ij}J_{i'j})^{-1/2}\eta_j\sqrt{1-\eta_j^2}\,\delta_{j,j'}\langle f_i^\nu|\tilde{L}_{3\xi}|f_{i'}^{\nu'}\rangle(\delta_{mm'+1}+\delta_{m'm+1})$$
$$+ \frac{i}{2}(J_{ij}J_{ij'})^{-1/2}(hx_i+1)\sqrt{hx_i(hx_i+2)}\,\delta_{i,i'}\langle g_j^\nu|\tilde{L}_{3\eta}|g_{j'}^{\nu'}\rangle(\delta_{mm'+1}+\delta_{m'm+1})$$
$$+ \frac{i}{4}\frac{(hx_i+1)\eta_j}{\sqrt{hx_i(hx_i+2)(1-\eta_j^2)}}\delta_{ii'}\delta_{jj'}(m+m')(\delta_{mm'+1}-\delta_{m'm+1}), \tag{A12}$$

where for $i \neq i'$

$$\langle f_i^0|\tilde{L}_{3\xi}|f_{i'}^1\rangle = (-1)^{i+i'}\frac{hx_i+hx_{i'}+4}{2h(x_i-x_{i'})}\sqrt{\frac{hx_i}{hx_{i'}+2}}, \tag{A13}$$

$$\langle f_i^1|\tilde{L}_{3\xi}|f_i^0\rangle = -\langle f_{i'}^0|\tilde{L}_{3\xi}|f_i^1\rangle, \tag{A14}$$

for $i = i'$

$$\langle f_i^0|\tilde{L}_{3\xi}|f_i^1\rangle = \frac{hx_i+1}{\sqrt{hx_i(hx_i+2)}}, \tag{A15}$$

$$\langle f_i^1|\tilde{L}_{3\xi}|f_i^0\rangle = -\langle f_i^0|\tilde{L}_{3\xi}|f_i^1\rangle, \tag{A16}$$

for $j \neq j'$

$$\langle g_j^0|\tilde{L}_{3\eta}|g_{j'}^1\rangle = (-1)^{i+i'}\frac{\sqrt{1-\eta_j^2}}{\eta_j-\eta_{j'}}, \tag{A17}$$

$$\langle g_j^1|\tilde{L}_{3\eta}|g_{j'}^0\rangle = -\langle g_{j'}^0|\tilde{L}_{3\eta}|g_j^1\rangle, \tag{A18}$$

and for $j = j'$

$$\langle g_j^0|\tilde{L}_{3\eta}|g_j^1\rangle = -\frac{\eta_j}{\sqrt{1-\eta_j^2}}, \tag{A19}$$

$$\langle g_j^1|\tilde{L}_{3\eta}|g_j^0\rangle = -\langle g_j^0|\tilde{L}_{3\eta}|g_j^1\rangle. \tag{A20}$$

The above matrix representation applies to both (decoupled) $\pi_3 = \pm 1$ symmetry blocks, when $m(m') = 1, 2, \ldots M$. In the case of $\pi_3 = 1$, the $m(m') = 0$ states are also involved and the only correction is that all matrix elements connecting states with $m = 0(1)$ and $m' = 1(0)$ should be multiplied by a factor of $\sqrt{2}$.

[1] E. A. Solov'ev, Sov. Phys. JETP. **54**, 893 (1981).

[2] R. McCarroll and D. S. F. Crothers, Adv. At. Mol. Opt. Phys. **32**, 253 (1994).

[3] E. A. Solov'ev, Theor. Mat. Phys. (USSR) **28**, 575 (1976).

[4] E. A. Solov'ev, Sov. J. Nucl. Phys. **35**, 136 (1982).

[5] E. A. Solov'ev, Sov. Phys. Usp. **32**, 228 (1989).

[6] V. V. Serov, V. L. Derbov, B. B. Joulakian, and S. I. Vinitsky, Phys. Rev. A **75**, 012715 (2007).

[7] E. Y. Sidky and B. D. Esry, Phys. Rev. Lett. **85**, 5086 (2000).

[8] A. Hamido, J. Eiglsperger, J. Madronero, F. Mota-Furtado, P. O'Mahony, A. L. Frapiccini, and B. Piraux, Phys. Rev. A **84**, 013422 (2011).

[9] T. P. Grozdanov and E. A. Solov'ev, Phys. Rev. A **42**, 2703 (1990).

[10] J. Macek, J. Phys. B **1**, 831 (1968).

[11] C.-N. Liu, A.-T. Le, T. Morishita, B. D. Esry, and C. D. Lin, Phys. Rev. A **67**, 052705 (2003).

[12] E. A. Solov'ev and S. I. Vinitsky, J. Phys. B **18**, L557 (1985).

[13] T. P. Grozdanov and E. A. Solov'ev, Eur. Phys. J. D **6**, 13 (1999).

[14] T. P. Grozdanov and E. A. Solov'ev, Phys. Rev. A **44**, 5605 (1991).

[15] E. A. Solov'ev, Physics Essays **25**, 27 (2012).

[16] M. Vincke and D. Baye, J. Phys. B: At. Mol. Opt. Phys. **39**, 2605 (2006).

[17] D. Baye, A. J. de ter Beerst, and J.-M. Sparenberg, J. Phys. B: At. Mol. Opt. Phys. **42**, 225102 (2009).

[18] D. Baye and P.-H. Heenen, J. Phys. A: Math. Gen. **19**, 2041 (1986).

[19] M. Abramowitz and I. A. Stegun, *Handbook of Mathematical Functions* (Dover, New York, 1965).

[20] J. Neumann and E. Wigner, Phys. Zs. **30**, 467 (1929).

[21] H. Wei, J. Chem. Phys. **106**, 6885 (1997).

[22] K. Willner, O. Dulieu, and F. Masnou-Seeuws, J. Chem. Phys. **120**, 548 (2004).

[23] E. A. Solov'ev and O. I. Tolstikhin, J. Phys. B: At. Mol. Opt. Phys. **34**, L439 (2001).

[24] N. S. Simonović and E. A. Solov'ev, Phys. Rev. A **87**, 052503 (2013).